41. C. Th. J. Alkemade, Tj. Hollander, W. Snelleman, P. J. Th. Zeegers, *Metal Vapours in Flames* (Pergamon, Oxford, 1982).
42. T. Tsuji, *Astron. Astrophys.* **23**, 411 (1973).
43. P. Pesch, *Astrophys. J.* **174**, L155 (1974).
44. C. W. Bauschlicher, Jr., S. R. Langhoff, T. C. Steimle, J. E. Shirley, *J. Chem. Phys.* **93**, 4179 (1990).
45. S. Drapatz, L. Haser, K. W. Michel, *Z. Naturforsch. Teil A* **29**, 411 (1974).
46. E. Murad, W. Swider, S. W. Benson, *Nature* **289**, 273 (1981); S. C. Lin and G. C. Reid, *Geophys. Res. Lett.* **6**, 283 (1979).
47. E. Murad, *J. Chem. Phys.* **75**, 4080 (1981).
48. J. M. Brom, Jr., and W. Weltner, Jr., *ibid.* **77**, 2057 (1982); *ibid.* **78**, 6611 (1983).
49. C. W. Bauschlicher, Jr., S. R. Langhoff, H. Partridge, *ibid.* **84**, 901 (1986).
50. J. V. Ortiz, *ibid.* **92**, 6728 (1990).
51. M. Menzinger, *Adv. Chem. Phys.* **42**, 1 (1980).
52. W. H. Breckenridge and H. Umemoto, *ibid.* **50**, 325 (1982).
53. P. J. Dagdigian and M. L. Campbell, *Chem. Rev.* **87**, 1 (1987).
54. B. Simard, W. J. Balfour, M. Vasseur, P. A. Hackett, *J. Chem. Phys.* **93**, 4481 (1990).
55. E. S. J. Robles, A. M. Ellis, T. A. Miller, *Chem. Phys. Lett.* **178**, 185 (1991).
56. J. B. West, R. S. Bradford, J. D. Eversole, C. R. Jones, *Rev. Sci. Instrum.* **46**, 164 (1975).
57. P. F. Bernath, B. Pinchemel, R. W. Field, *J. Chem. Phys.* **74**, 5508 (1981).
58. S. F. Rice, H. Martin, R. W. Field, *ibid.* **82**, 5073 (1985).
59. T. Törring, W. E. Ernst, J. Kändler, *ibid.* **90**, 4927 (1989).
60. J. V. Ortiz, *Chem. Phys. Lett.* **169**, 116 (1990).
61. ———, *J. Am. Chem. Soc.* **113**, 1102 (1991).
62. ———, *ibid.*, p. 3593.
63. A. M. Golub, H. Kohler, V. V. Skopenko, *Chemistry of the Pseudohalides* (Elsevier, Amsterdam, 1986).
64. K. K. Joshi, P. L. Paulson, A. R. Qazi, W. H. Stubbs, *J. Organomet. Chem.* **1**, 471 (1964).
65. E. S. J. Robles, A. M. Ellis, T. A. Miller, paper RB4, presented at the Forty-Sixth International Symposium on Molecular Spectroscopy, Columbus, Ohio, 17 to 21 June 1991.
66. N. N. Greenwood and A. Earnshaw, *Chemistry of the Elements* (Pergamon, Oxford, 1984).
67. A. M. Denis, J. D. Korp, I. Bernal, R. A. Howard, J. L. Bear, *Inorg. Chem.* **22**, 1522 (1983).
68. I thank my students and collaborators, C. Brazier, A. M. R. P. Bopegedera, L. O'Brien, W. T. M. L. Fernando, S. Kinsey-Nielsen, S. Pianalto, R. Hailey, M. Douay, R. Ram, and C. Jarman, for their invaluable contributions to the work summarized here. This work was supported by the NSF, Petroleum Research Fund, Office of Naval Research, Research Corporation, Natural Science and Engineering Research Council of Canada, and the Astronautics Laboratory, Edwards Air Force Base. I acknowledge support as an Alfred P. Sloan Fellow and a Camille and Henry Dreyfus Teacher-Scholar. I thank K. Walker and A. Tang for assistance with the figures.

Stress Fields of the Overriding Plate at Convergent Margins and Beneath Active Volcanic Arcs

K. DENISE APPERSON

Tectonic stress fields in the overriding plate at convergent plate margins are complex and vary on local to regional scales. Volcanic arcs are a common element of overriding plates. Stress fields in the volcanic arc region are related to deformation generated by subduction and to magma generation and ascent processes. Analysis of moment tensors of shallow and intermediate depth earthquakes in volcanic arcs indicates that the seismic strain field in the arc region of many convergent margins is subhorizontal extension oriented nearly perpendicular to the arc. A process capable of generating such a globally consistent strain field is induced asthenospheric corner flow below the arc region.

CONVERGENT PLATE MARGINS PRODUCE THE WIDEST VARIATION in deformation styles of any tectonic environment. Principal tectonic features at convergent margins include the subducting plate and associated sediments, the interplate shear zone, and the overriding plate. The overriding plate may possess a forearc with a large deforming accretionary wedge (*1*), forearc basins and highs, a strong backstop beneath the forearc (*2*), a volcanic arc, and a backarc (*3*) (Fig. 1). Tectonic stress fields within the heterogenous convergent margin system are complicated as a result of local to regional variations in material properties, geometry of the plate boundary, and plate motions. Knowledge of regional stress fields is important for understanding how subduction and collision affect deformation of the overriding plate. In particular, characterization of stress fields in the volcanic arc region provides a link between forearc and backarc deformation and can help us understand magma generation and ascent processes.

A volcanic arc is a primary product of plate subduction and is a feature common to all margins where convergence is faster than a few centimeters per year and the dip of the subducting plate is not horizontal at depths of about 100 km. One of the most notable features of volcani arcs is their location, on average, 125 km above the Wadati-Benioff zone c of seismicity in the subducting plate (*4, 5*). The spacing of volcanic centers varies considerably from arc to arc and along strike of a single arc, although through millions of years of activity many volcanic arcs exhibit a relatively regular and surprisingly narrow width of about 50 km (*4*).

Earthquakes beneath active volcanic arcs can occur in arc crust and lithosphere, possibly in the underlying asthenospheric wedge, and in the upper parts of the Wadati-Benioff zone (at depths around 100 to 200 km). In this article, I use strain information contained in summed earthquake moment tensors to characterize the seismic strain field of the volcanic arc region of overriding plates at active convergent margins. If we assume that the seismic strain fields are simply related to tectonic stress fields, we can examine the effects that subduction and magma generation processes have upon overriding plate deformation. As a context for interpretation of the data, I first review the general nature and controls of stresses in the overriding plate.

Tectonic Stress Fields and Deformation of Overriding Plates

In the 1970s, the conventional view was that subhorizontal compressive tectonic stresses were transmitted throughout the over-

The author is in the Department of Geological Sciences, University of Texas at Austin, Austin, TX 78713.

riding plate as a result of plate convergence and that the principal mode of deformation of the overriding plate was shortening parallel to the convergence direction. It is now thought that shortening directly due to convergence is localized at the front of the forearc region in the toe of the accretionary wedge (see Fig. 1) [for example, (*6*)]. In some cases the width of this active fold and thrust belt is only a few kilometers, as at Mariana, and in others it can be as wide as several tens of kilometers, as at Lesser Antilles.

Stress fields are often inferred from correlation between variables such as slab dip at depths of 100 km, age of the subducting slab, numbers of large interplate thrust earthquakes, direction and rate of convergence, absolute plate motions, and the presence or absence of physical features such as a large accretionary wedge or an actively spreading backarc (*7–9*) (Table 1). For example, large interplate shear zone earthquakes appear to be most abundant in areas where young, warm, buoyant plates are being rapidly subducted (*7*).

Numerical models of stress fields have been used to evaluate the processes responsible for the observed spectrum of deformation (*10*). Asthenospheric convection, changes in dip of the subducting slab, gravity and isostasy, and different rheological behaviors can be considered in such models. Most models indicate that the stress field in the forearc of the overriding plate is likely to be compressional and subhorizontal, in agreement with observation. However, both the results of numerical models and observations suggest that stress fields in other parts of the overriding plate are variable and complicated [for example, (*11*)].

Primary controls on tectonic stress fields of the overriding plate are intraplate stresses, such as due to trench suction, and boundary tractions generated by asthenopheric flow (Fig. 1). Viscous drag associated with the subducting plate induces asthenospheric convection in the corner between the plates (*12, 13*). In turn, this convection induces drag on the base of the overriding plate; the drag is enhanced as the dip of the subducting plate increases (*14*). The dip of the subducting slab can in turn be influenced by regional asthenospheric flow exerting pressure on both sides of the slab. Slab pull on the subducting plate, a result of the plate sinking under its own weight, causes rollback of the subducting plate from the trench (*15*) and results in an intraplate force that couples the forearc to the descending plate (*16*). Intraplate forces are also provided by isostatic effects associated with uplift and downwarping of the plates near the trench region (*11*).

The balance of intraplate forces and boundary shear forces is critical. Backarc extension may result when the force balance on the forearc region is such that it moves oceanward faster than the rest of the overriding plate. In contrast, shortening may occur in the backarc or forearc when the forearc region moves more slowly than the rest of the overriding plate. Absolute plate motions of the subducting and overriding plates will also affect this force balance (*17*). Deformation within the arc will also play an important role in the force balance of the overriding plate.

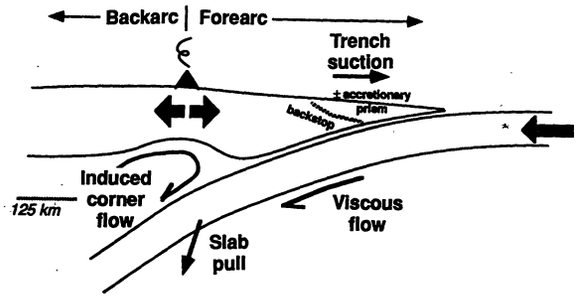

Fig. 1. Principal tectonic features of the convergent margin system. A large accretionary prism may or may not be present because the rates of sediment accumulation, erosion, and subduction will vary through time. The shape and composition of the backstop is not well known (*2*). Tectonic stress fields in the overriding plate result from a balance between intraplate stresses such as trench suction and boundary tractions caused by asthenospheric flow. Corner flow is induced in the asthenosphere wedge above the subducting plate by viscous drag on the subducting slab (*12, 13*). The seismic extension in the volcanic arc discussed in this paper is denoted by the two black arrows.

Seismicity and Volcanic Arcs

Directly beneath volcanic arcs, earthquakes occur from near the surface to depths of more than 200 km. Shallow crustal events (<50 km) may be associated with magma migration and intrusion by the mechanism of magma-driven elastic fracture propagation (*18*). Most of the largest events occur at intermediate depths between about 50 and 170 to 200 km. The location of the deeper events is problematic. Velocity anomalies associated with cold subducting slabs can result in mislocation of earthquakes in the vicinity of a convergent margin (*19, 20*). Thus, these events could be located in lower arc lithosphere, in the asthenosphere wedge above the subducting slab, or in the Wadati-Benioff zone. Workers who have examined seismicity within several areas have noted that the astherospheric wedge beneath the arc may be aseismic (*20–25*).

The mechanisms of the intermediate-depth volcanic arc events are

Table 1. Selected physical characteristics of convergent margin subregions. Two convergent margin classifications that are related to tectonic stress fields in the overriding plate are shown for comparison. The first is based on the size of the largest interplate shear zone thrust earthquake (*7*). Margins with many large interplate thrust events are thought to have strongly coupled overriding and subducting plates. The second classification is based on combined strain and stress fields of the overriding plate (*8*). The orientation of the volcanic line (VL) is determined by a least squares best fit line through active volcanoes in each subregion. The azimuth of the normal to the volcanic line is shown (VLN). Also listed is the minimum distance between the volcanic line and the plate boundary as determined from cross sections (Fig. 5). The obliquity of convergence is based on the NUVEL-1 plate motion model (38). The obliquity is defined to be the angle between the direction of convergence of the subducting plate and the normal direction to the volcanic line. N, north; C, central; S, south.

	Region	OP crust*	Coupling†	VLN	VL dist. (km)	Obliquity
1	E. Aleutians	O	S 4	161°	125	69°
2	C. Aleutians	O	S 4	178°	125	85°
3	Kamchatka	O/C	S 5	115°	175	38°
4	N. Kuriles	C	S 5	132°	150	59°
5	S. Kuriles	C	S 5	155°	225	85°
6	Japan	C	I 6	113°	250	41°
7	Bonin	O	W 2	78°	175	43°
8	N. Marianas	O	W 1	50°	150	17°
9	C. Marianas	O	W 1	82°	200	52°
10	C. Tonga	O	I 1	109°	250	20°
11	S. Tonga	O	I 1	108°	175	19°
12	Kermadec	O	I 1	110°	‡	20°
13	Sumatra	C	I 5	53°	275	30°
14	Java	O/C	W 5	14°	250	6°
15	N. Chile	C	S 7	95°	300	28°
16	C. Chile	C	S 7	100°	‡	23°
17	S. Chile	C	S 5	110°	225	14°

*Crust type of overriding plate (OP): O = oceanic, C = continental, O/C = transitional or both (*4, 8*). †Convergent margin classifications. S = strong coupling, I = intermediate, W = weak (*7*). 1 = strongly tensional (active backarc spreading), 2 = tensional (slow backarc spreading), 3 = mildly tensional, 4 = neutral, 5 = mildly compressional, 6 = moderately compressional, 7 = strongly compressional (*8*). ‡Kermadec and C. Chile subregions do not have substantial recent volcanic activity.

also problematic because of the uncertainties in location. It has been proposed that the intermediate-depth events are due to stress concentrations in colder stronger material in contact with weak melt zones beneath active volcanoes (*21, 26*). The intermediate-depth events might be evidence of continuity in the magma system from depths of about 150 km to the surface if pressure fluctuations transmitted throughout the system by a volcanic eruption triggered the earthquakes (*23*). Although epicenters are generally within 50 km of active volcanoes (*27*), association of large intermediate-depth earthquakes with individual volcanic eruptions is usually ambiguous, in part because of the short length of time sampled by earthquake catalogs compared to the repeat time of large eruptions (*21, 23*).

Analysis of Earthquake-Related Deformation

The earthquake moment tensor is related to a seismic strain tensor, which represents deformation due to seismic activity. In this paper, "seismic strain" refers to deformation resulting from earthquake activity. My method of analysis consists of summing the moment tensors of earthquakes in a specific region to obtain information on the distributed seismic deformation (*28*). Discussion of "summed" sources below refers to various characteristics of the average moment tensor obtained by summing the tensors of a group of earthquakes. The primary data source for this study is the Harvard centroid moment tensor (CMT) catalog which contains 8118 events that occurred between 1978 and September 1989 (*29, 30*).

The seismic moment tensor **M** can be related to a seismic strain tensor because it relates amplitudes and directions of seismic waves leaving the earthquake source to their displacement. Like a strain tensor, the three-by-three symmetric earthquake moment tensor is completely described by the values of its three principal moments m_T, m_B, and m_P, and the orientations of its three principal axes, the *T*, *B*, and *P* axes [for more information, see (*31, 32*)]. The seismic moment *Mo*, a scalar quantity with units of dyne centimeters, can be used as a measure of the size of an event and is expressed in terms of the three principal moments by

$$Mo = \sqrt{\frac{m_T^2 + m_B^2 + m_P^2}{2}} \quad (1)$$

In a double-couple model of an earthquake source, it is assumed that material deformation near the source can be represented by slip on a planar fault. For a pure double-couple earthquake, $m_T = 1.0$, $m_P = -1.0$, and $m_B = 0.0$. Traditional first-motion "beachball" plots are focal mechanisms of double-couple events. Focal mechanisms can be determined from the moment tensor by the orientations of the three principal axes. Although the double-couple source model is successful in explaining the general displacement patterns of most earthquakes, many earthquakes contain non–double couple components that represent more complex patterns of seismic strain (*33, 34*). When analyzing regional strain patterns, these components should also be considered.

The parameter f_{ndc} measures the deviation of an earthquake source from a pure double-couple event and is defined in terms of the principal moments by

$$f_{ndc} = \frac{|m_B|}{\mathrm{MAX}(|m_T|,|m_P|)} \quad (2)$$

It is the ratio of the absolute value of the intermediate principal moment to the absolute value of the largest of the remaining two moments; f_{ndc} equals 0.0 for a pure double-couple event (because $m_B = 0.0$) and 0.5 for one particular type of event with no double-couple component (Fig. 2). The value of f_{ndc} for a typical earthquake in the CMT catalog is 0.1, indicating that the typical source contains about 20% non–double couple components (*30, 35*).

The sum of the moment tensors M_i of a group of N earthquakes occurring in a volume V is related to an average seismic strain tensor ε according to

$$\varepsilon = \frac{1}{2\mu V} \sum_{i=1,N} \mathbf{M}_i \quad (3)$$

where μ is the rigidity of the material (*36*). Accordingly, there is a correspondence between the directions of principal strain and the P, T, and B axes.

The seismic consistency C_s is a statistic that measures how similar earthquakes in a group are to one another (*32*). It is defined by

$$C_s = \frac{Mo_{sum}}{\sum_{i=1,N} Mo_i} \quad (4)$$

where Mo_i and Mo_{sum} are the scalar moments of the ith moment tensor $\mathbf{M}_i$ and the summed moment tensor $\mathbf{M}_{sum} = \mathbf{M}_1 + \mathbf{M}_2 + \ldots$

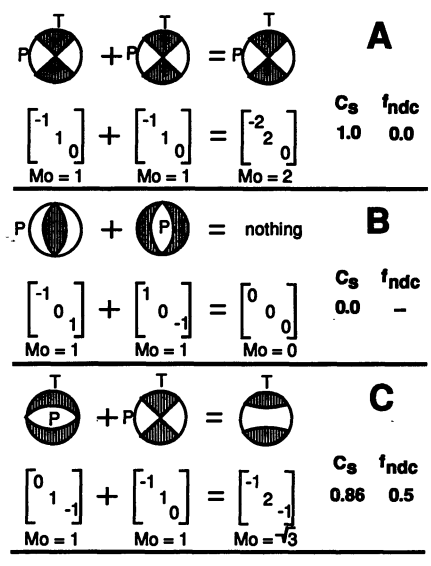

Fig. 2. A demonstration of moment tensor summation. Lower hemisphere equal area focal mechanism projections (beachballs) are determined from the T, B, and P principal axes of the earthquake moment tensor. Focal mechanisms can also be determined for earthquakes with non–double couple components. The orientations of the T, B, and P principal axes of the non-double couple focal mechanism are the same as if a focal mechanism was plotted with the assumption that $m_B = 0.0$, but the nodal planes of double couple beachballs become curved nodal surfaces for the non–double couple mechanism. Focal mechanism quadrants that represent compressional motion at the earthquake source are shaded. The B axis lies at the intersection of the nodal planes, which are surfaces of no compressional wave motion at the earthquake source. Only the values of the principal moments are shown in the moment tensors below the focal mechanisms. Off-diagonal terms in these examples are zero. The P axis is associated with the smallest principal moment, the T axis with the largest principal moment, and the B axis with the intermediate valued moment. The seismic moment *Mo* (Eq. 1) is shown below each tensor. The value of the seismic consistency C_s (Eq. 4) and the non–double couple ratio f_{ndc} (Eq. 2) are calculated for each summed source. (**A**) If all earthquakes in a group have identically oriented moment tensors, C_s will be equal to 1.0; f_{ndc} is zero because pure double couple sources have been used in the example. (**B**) If the tensors of a normal-type and a thrust-type earthquake with parallel B axes and perpendicular P or T axes are summed, the sources cancel each other and the seismic consistency is zero. (**C**) It is possible to produce an event containing no double couple components by adding two appropriately oriented pure double couple events. In this case the result is a pure compensated linear vector dipole (CLVD) source [for example (*30, 34*)]. There is evidence that complexity of the earthquake source in time and space causes many of the known events with a large component of CLVD (*33*). In this example, f_{ndc} has a maximum value of 0.5. Although the total seismic deformation is more complex than simple slip on a planar fault, the value of C_s is relatively high.

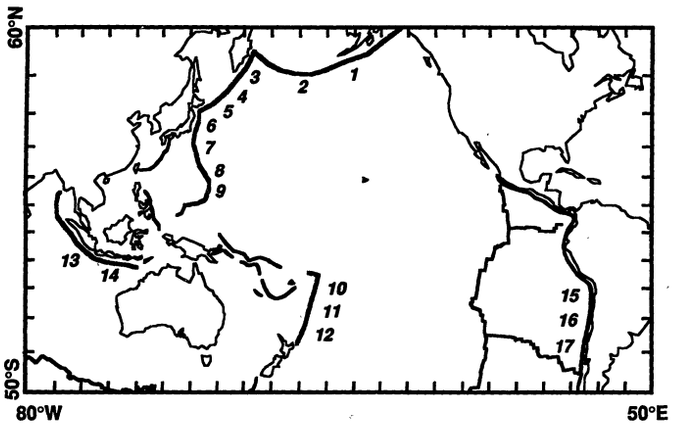

Fig. 3. Map of the circum-Pacific region with plate boundaries. Convergent margins analyzed are keyed to numbered subregions in Table 1.

M_n, respectively. C_s ranges from 0.0 to 1.0, and is close to 1.0 if the earthquakes in a group are similar (Fig. 2). Including in a sum even a few events whose sources are very different from the rest of a group will degrade the consistency. If one event in a group is much larger than the others, it is helpful to normalize the moment tensors, M_i/Mo_i. In this way, C_s for the normalized tensors is similar to a visual estimate of whether several plotted mechanisms are alike or different (*32*).

The active convergent margins included in this study represent about 60% of the total length of the world's convergent margin plate boundaries (Fig. 3) (*37*). The convergent margins chosen possess a range of physical and geometrical characteristics such as convergence rate, convergence direction (*38*), and age and dip of the slab. All of these factors have been linked to tectonic stress fields of the overriding plate.

Out of 8118 total events in the CMT catalog, 326 events with focal depths less than 200 km can be associated with the active volcanic arcs selected for study (Fig. 3 and Table 1). I used both source characteristics and location to identify these events (*39*). For each convergent margin, I plotted on cross sections all earthquakes with focal depths less than 200 km that were located about 400 to 500 km arcward of the plate boundary (*40, 41*) (Fig. 4). Interplate shear zone thrust earthquakes, events in the Wadati-Benioff zone, as well as events in the overriding plate, were included in the initial analysis. I then summed the moment tensors of various groups of earthquakes in each cross section, and separated groups of events with similar source characteristics, measured in part by the seismic consistency C_s. Boundaries of subgroups, defined by depth and distance from the plate boundary, were chosen to maximize the number of earthquakes in each group. The term "volcanic arc events" refers to those groups of similar earthquakes, located beneath volcanic arcs at a range of depths, that possess source characteristics that are different from events such as those in the interplate shear zone. Although moment tensor sums were performed for all earthquakes and all reasonable subgroups in every cross section, this paper focuses on the analysis of the volcanic arc events.

In general, volcanic arc events can be broken into two groups, one containing events at depths less than 50 km (shallow) and the other containing events located at depths 100 km and greater (intermediate) (Table 2). Nine out of 17 convergent margin subregions had events in the shallow group (Table 2). Almost all margins had events in the intermediate-depth group. The depth region between about 50 and 100 km is notably aseismic in many regions, although this may be an artifact of mislocations (*19*). I discuss results from three margins, Mariana, Sumatra-Java, and Kamchatka-Kuriles, as examples (Fig. 4).

In the north and central Mariana subregions (Fig. 5A), summed

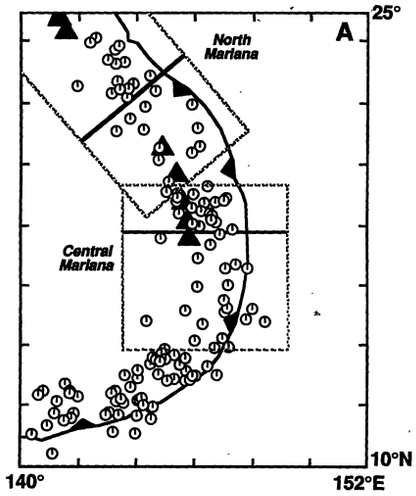

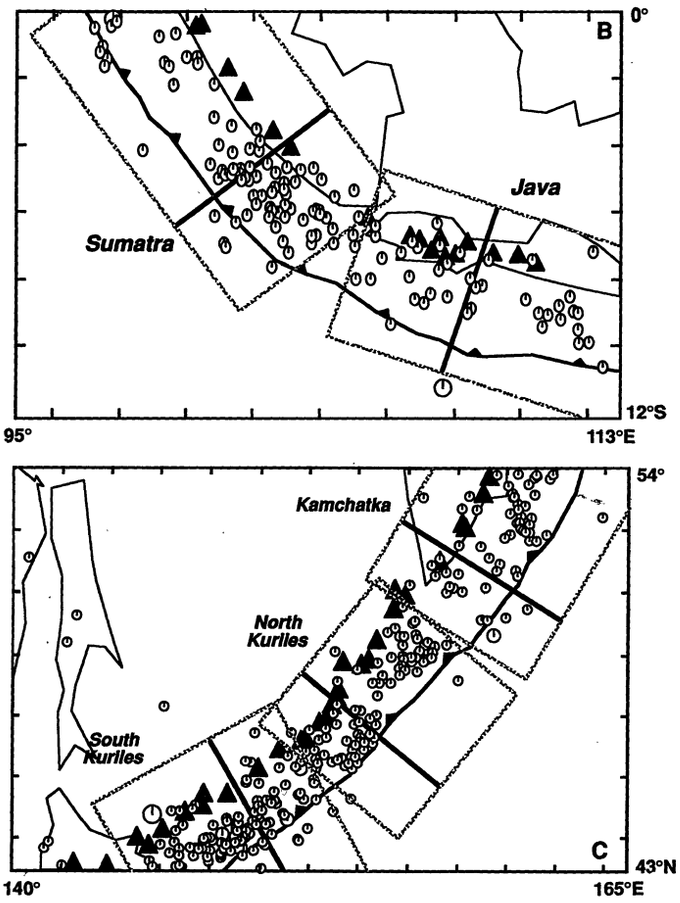

Fig. 4. Regional earthquake location maps. Because some convergent margins are thousands of kilometers long, the azimuth of the plate boundary and volcanic line change significantly. I subdivided many of the longer margins such as Kamchatka-Kuriles to take this into account. (**A**) Tectonic map of the Mariana convergent margin. Circles are earthquakes with focal depths less than 200 km; larger symbols indicate events with seismic moments ≥ 10^{26} dyne cm. Selected recently active volcanoes are marked by black triangles. The toothed line marks the plate boundary. The location of cross sections, oriented normal to the volcanic line, are shown by the heavy lines. The boxes outlined by dotted lines enclose all events included on each cross section. (**B**) Tectonic map of the Sumatra and Java convergent margins. (**C**) Tectonic map of the Kamchatka and Kuriles convergent margin. The margin is divided because of small changes in the azimuth of the volcanic line and to spread the large number of events out between several sections for convenience.

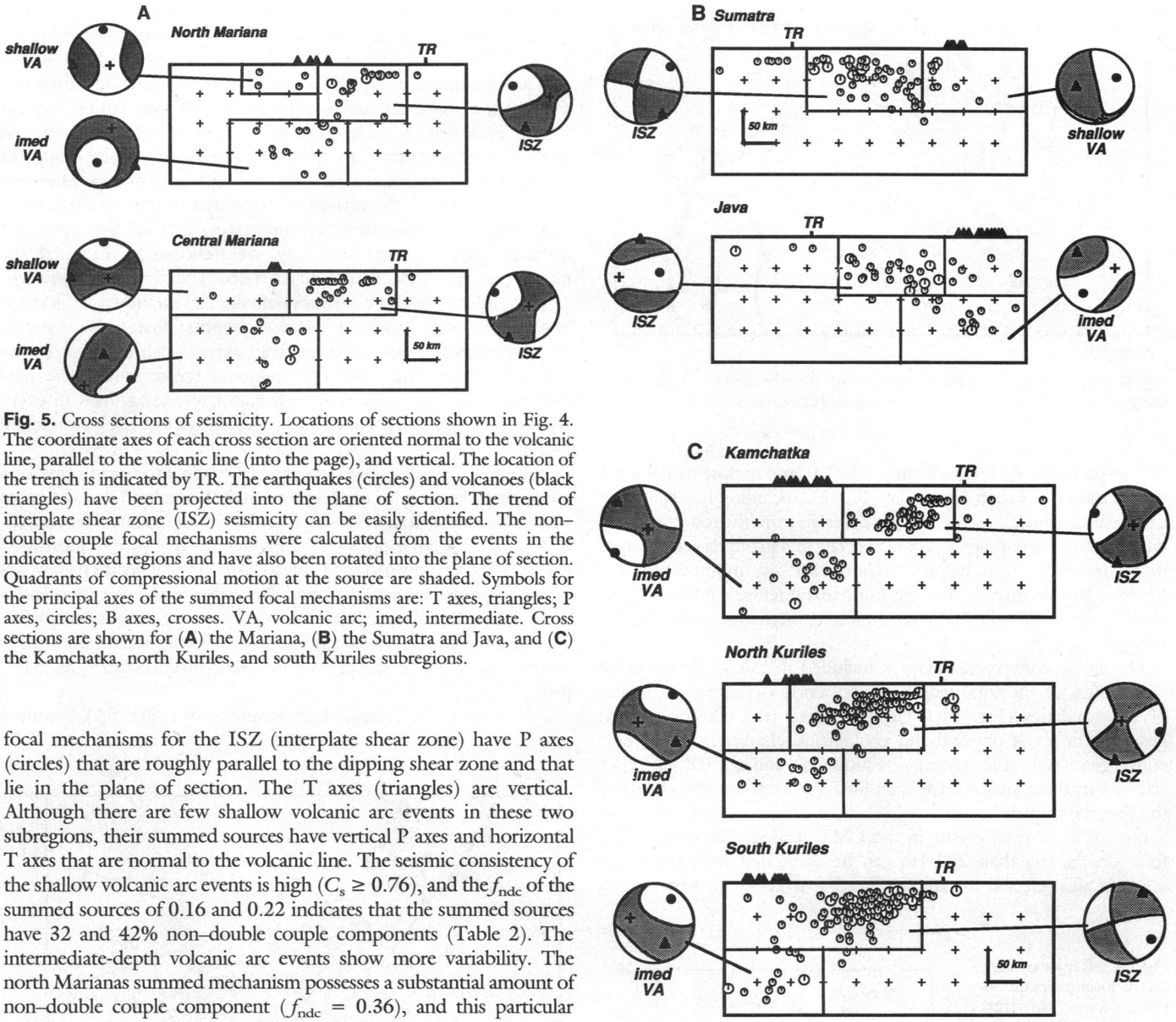

Fig. 5. Cross sections of seismicity. Locations of sections shown in Fig. 4. The coordinate axes of each cross section are oriented normal to the volcanic line, parallel to the volcanic line (into the page), and vertical. The location of the trench is indicated by TR. The earthquakes (circles) and volcanoes (black triangles) have been projected into the plane of section. The trend of interplate shear zone (ISZ) seismicity can be easily identified. The non–double couple focal mechanisms were calculated from the events in the indicated boxed regions and have also been rotated into the plane of section. Quadrants of compressional motion at the source are shaded. Symbols for the principal axes of the summed focal mechanisms are: T axes, triangles; P axes, circles; B axes, crosses. VA, volcanic arc; imed, intermediate. Cross sections are shown for (**A**) the Mariana, (**B**) the Sumatra and Java, and (**C**) the Kamchatka, north Kuriles, and south Kuriles subregions.

focal mechanisms for the ISZ (interplate shear zone) have P axes (circles) that are roughly parallel to the dipping shear zone and that lie in the plane of section. The T axes (triangles) are vertical. Although there are few shallow volcanic arc events in these two subregions, their summed sources have vertical P axes and horizontal T axes that are normal to the volcanic line. The seismic consistency of the shallow volcanic arc events is high ($C_s \geq 0.76$), and the f_{ndc} of the summed sources of 0.16 and 0.22 indicates that the summed sources have 32 and 42% non–double couple components (Table 2). The intermediate-depth volcanic arc events show more variability. The north Marianas summed mechanism possesses a substantial amount of non–double couple component (f_{ndc} = 0.36), and this particular group has a low value of C_s of 0.64 (Table 2).

The Sumatra and Java cross sections are shown in Fig. 5B. The trace of the ISZ in Java is more diffuse than for the Sumatra section. The intermediate-depth volcanic arc events in the Java section produce a near vertical T axis (triangle) in the plane of section. Although these events produce a sum with substantial non–double couple components (f_{ndc} = 0.28), the seismic consistency is fairly high (0.71, Table 2). The six shallow volcanic arc events in Java have widely varying sources and produce such a low seismic consistency that summing the moment tensors is not warranted. The summed source for ISZ events in Sumatra has a subhorizontal P axis that is in the plane of section. The shallow volcanic arc events produce a summed mechanism with horizontal P and T axes both going into the plane of section at roughly 30°, and a vertical B axis (cross). This summed source has a high seismic consistency (0.94) and is close to being double couple (Table 2).

The Kamchatka and north and south Kuriles subregions have similar summed mechanisms for ISZ events (Fig. 5C). The P axes are horizontal roughly parallel to the ISZ, and the T axes are vertical. All three of these subregions had intermediate-depth volcanic arc earthquakes whose summed mechanisms have substantial amounts of non–double couple components ($f_{ndc} \geq 0.28$, Table 2). The low consistency C_s of these three groups (≤ 0.62) indicates that the earthquakes included in the sums have diverse source types and orientations. Rearranging the boundaries of the earthquake subgroups in these cross sections did not improve the consistency.

Seismic Strain in Volcanic Arcs

The systematic source patterns of the volcanic arc earthquakes indicate that the strain field in the volcanic arc region is coherent. This seismic strain field is systematically related to the orientation of the volcanic line. The highly consistent orientation of the T axes of summed volcanic arc earthquakes in two-thirds of the margins studied indicates that the seismic strain field to depths of about 150 km in the volcanic arc region of the overriding plate is subhorizontal extension oriented nearly perpendicular to the arc (Fig. 6) (*42*). I have interpreted the dominant seismic strain field as extension normal to the arc rather than shear parallel to the arc. Although the summed sources include both strike-slip type with nearly vertical B axes and oblique-normal type with nearly vertical P axes, only 7 out

of 23 subregions (counting both shallow and intermediate) produced strike-slip summed sources.

A second, less coherent strain field is present in about one-third of the convergent margin subregions studied in which T axes of the summed sources are closer to being parallel to the volcanic line rather than perpendicular. However, the low values of seismic consistency in these subregions (Table 2) and scattered orientations of the summed sources (Fig. 6) suggest that there is a large amount of individual source variability.

The relation between the summed sources and the orientation of the volcanic line can best be seen by rotation of the summed moment tensors into a coordinate system that is relative to the volcanic line so that one coordinate axis is parallel to it, one axis is normal, and the third axis is vertical (Fig. 6). In seven out of nine convergent margin subregions with shallow volcanic arc events, the summed moment tensors have T axes oriented within 25° of the normal to the volcanic line (Shallow 1, Fig. 6A). Five of these seven subregions have T axes with dips less than 10°, that is, nearly horizontal. Three regions (Kermadec, south Tonga, and Bonin) have strike-slip type summed sources, determined by their nearly vertical B axes. The nearly vertical average P axes indicate that three other regions (central Mariana, north Mariana, and central Tonga) have normal type sources. The remaining two convergent margin subregions with shallow volcanic arc events (Japan and Sumatra) have summed moment tensors with T axes oriented more than 48° from the normal to the volcanic line (Shallow 2, Fig. 6A). The near-vertical dips of the B axes of these summed tensors indicate that the summed sources are of strike-slip type. All subregions with shallow volcanic arc events have high values of seismic consistency ($C_s \geq 0.70$). The values of f_{ndc} for shallow events range from 0.04 for Sumatra to 0.42 for south Tonga (Table 2), and show no consistent relation to orientation of the seismic strain.

The situation for intermediate-depth volcanic arc events is quite similar. In the first group, containing 7 out of 14 subregions, the summed tensors have T axes oriented within 28° of the normal to the volcanic line (Intermediate 1, Fig. 6B). These summed sources are interpreted to be an oblique-normal type of seismic strain on the basis of the near horizontal B axes and the gently dipping (about 35°) P axes. The T axes of these summed tensors dip between 22° and 45°, greater than for the related shallow group. The remaining seven convergent margin subregions with intermediate-depth volcanic arc events have summed tensors with loosely clustered T axes oriented more than 30° from the normal to the volcanic line (Intermediate 2, Fig. 6B). Three regions out of these seven (Kermadec, central Marianas, and central Chile) have T axes within 15° of parallel to the volcanic line. The P axes of the summed sources of the Intermediate 2 group lie on a girdle oriented roughly normal to the volcanic line, whereas the T axes are loosely clustered on a girdle oriented more parallel to the volcanic line. Two regions (central Marianas and Kermadec) produce strike-slip type summed sources as determined by the more vertical B axes, and the rest have more oblique-normal type sources with steeper P axes. The dips of the T axes of the Intermediate 2 group are greater than 29°. The seismic consistency of the Intermediate 1 group is generally high, but values of C_s for the Intermediate 2 group vary widely (Table 2). Although

Table 2. Results of moment tensor analysis of volcanic arc earthquakes. The subregions are grouped as in Fig. 7.

	Region	NEQ*	Depth† (km)	Moment‡ (10^{26} dyne cm)	C_s	f_{ndc}
			Shallow 1			
2	C. Aleutians	35	0 to 50	1.8	0.86	0.19
7	Bonin	20	0 to 50	2.8	0.70	0.27
8	N. Marianas	4	0 to 50	0.04	0.76	0.22
9	C. Marianas	3	0 to 50	0.03	0.87	0.16
10	C. Tonga	16	0 to 50	0.45	0.70	0.14
11	S. Tonga	13	0 to 50	0.62	0.91	0.42
12	Kermadec	12	0 to 75	0.92	0.81	0.29
			Shallow 2			
6	Japan	15	0 to 50	0.56	0.71	0.27
13	Sumatra	10	0 to 75	1.4	0.94	0.04
			Intermediate 1			
3	Kamchatka	12	100 to 200	0.44	0.59	0.28
7	Bonin	14	50 to 200	4.0	0.92	0.21
8	N. Marianas	12	100 to 200	0.57	0.64	0.32
10	C. Tonga	24	100 to 200	36.0	0.97	0.01
11	S. Tonga	19	50 to 200	1.0	0.82	0.06
14	Java	10	100 to 200	0.78	0.79	0.28
17	S. Chile	14	50 to 200	0.22	0.75	0.28
			Intermediate 2			
2	C. Aleutians	16	50 to 200	0.76	0.62	0.17
4	N. Kuriles	9	100 to 200	0.15	0.33	0.28
5	S. Kuriles	9	100 to 200	0.74	0.62	0.33
9	C. Marianas	11	50 to 200	0.78	0.88	0.16
12	Kermadec	4	100 to 200	0.04	0.50	0.12
15	N. Chile	35	100 to 200	4.1	0.46	0.18
16	C. Chile	9	50 to 200	0.22	0.75	0.28

*Number of events in specified subregion. †Depth range of events in subregion (kilometers). ‡Total seismic moment of group.

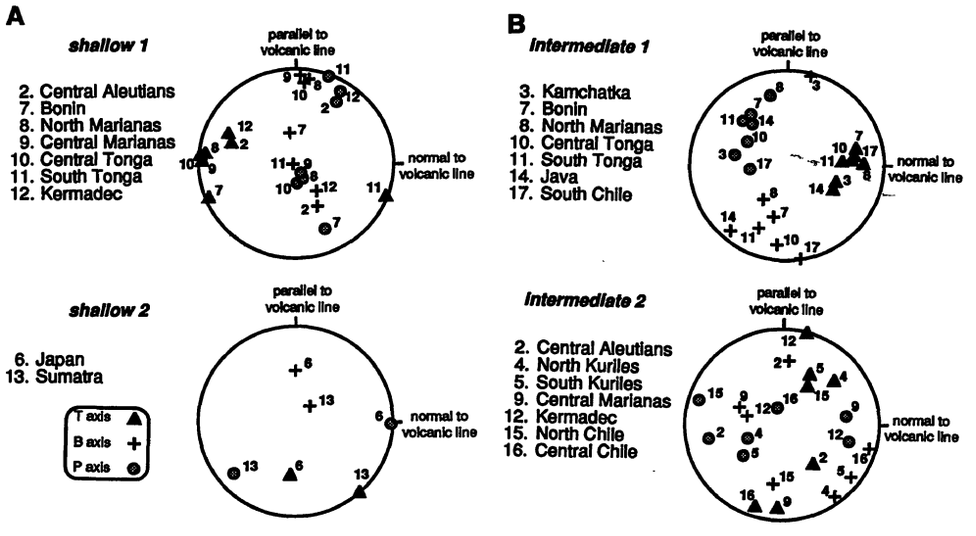

Fig. 6. (**A**) The T, B, and P principal axes of summed moment tensors from each convergent margin subregion in Table 2 rotated into a coordinate system that is relative to the volcanic line. Numbers next to each principal axis symbol correspond to numbered subregions to left (symbols as in Fig. 5). Subregions in Shallow 1 group have summed T axes within 25° of the normal to the volcanic line. Subregions in Shallow 2 group have summed T axes lying farther than 38° from the volcanic line normal. (**B**) Same as (A), but for intermediate-depth volcanic arc events. Subregions in Intermediate 1 group have summed T axes within 28° of normal to volcanic line. Subregions in Intermediate 2 group have summed T axes lying farther than 33° from the normal to the volcanic line.

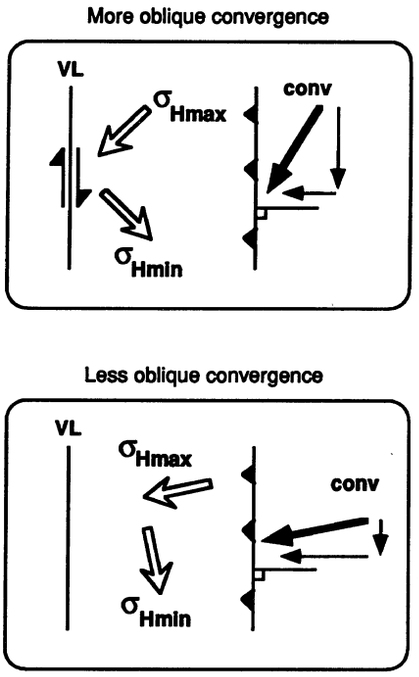

Fig. 7. Principal stresses in overriding plate predicted from decoupling models of oblique convergence. The models predict that the orientation of the stress field in the overriding plate will change as convergence obliquity changes. The convergence vector (conv) is decoupled into components normal and parallel to the plate boundary. The component parallel to the boundary is larger when the obliquity of convergence is greater. The maximum horizontal stress σ_{Hmax} would in this case be oriented at a smaller angle to the plate boundary and volcanic line (VL), resulting in strike slip deformation in the arc region [for example (*46*)].

the low values of seismic consistency in these convergent margin subregions indicates that source type and orientation are variable, the girdle patterns indicate that there is a systematic organization to the seismic strain. Just as for the shallow subregions, f_{ndc} for both intermediate-depth groups varies widely from 0.01 in central Tonga to 0.33 in south Kuriles, and there is no consistent relation to orientation of seismic strain (*43*).

Seismic Strain and Obliquity of Convergence

Knowledge of strain fields in the arc region can help us understand how subduction affects deformation in this part of the overriding plate. In particular, oblique convergence is frequently cited as a possible mechanism for variations in observed deformation styles and inferred stress fields at active convergent margins [for example (*44*)]. However, on the basis of the results of this study, the obliquity of convergence does not appear to have a consistent relation to the orientation of seismic strain in volcanic arcs.

It is generally assumed that oblique convergence of the subducting plate is decoupled into an underthrusting component that is normal to the plate boundary and a strike-slip component that is parallel to the plate boundary (*45*) (Fig. 7). The weak, long-lived volcanic arc is thought to be the locus of the strike-slip faults (*46*), although the parallel component could be taken up by oblique shear in the interplate shear zone or by deformation in the forearc. The Sumatra convergent margin is often cited as an example of the decoupling process [for example (*47*)].

Decoupling models of oblique convergence predict that at margins with more oblique convergence, the maximum horizontal tectonic stress σ_{Hmax} is at a small angle to the volcanic line and will produce strike-slip motion on an arc-parallel fault (*48*) (Fig. 7). If we assume a relation between seismic strain and tectonic stress, we can use the orientation of the summed earthquake moment tensors to test the decoupling hypothesis (Fig. 8). Variations in convergence obliquity appear to have no systematic influence on the orientation of seismic strain in the volcanic arc region. The preferred interpretation of the seismic strain field in the volcanic arc region is subhorizontal extension normal to the arc rather than shear parallel to the arc; this interpretation suggests that if strike-slip faults are commonly produced in the volcanic arc region by oblique convergence, they may either be aseismic or small.

Extension of Arcs and Magma Differentiation

Deformation and stress fields in the arc region affect magma generation and ascent. In particular, because magma ascent is controlled by buoyancy and thermal effects, extension of arc lithosphere has a direct effect on the height to which a magma body can ascend, and thus the amount and type of differentiation, such as crystal fractionation and crustal contamination, that operates (*49–51*). For example, in the central Aleutian arc, basaltic lavas from volcanoes located on highly extended crust show evidence of crystallization at shallow depths and did not undergo the crystal fractionation processes of basaltic lavas located on unextended crust (*52*). Magmas will also be modified during ascent through the lithosphere of the overriding plate [for example (*53–55*)].

The linear segmentation of many active arcs has also been related to extension of the arc lithosphere and results in variations in chemistry and volume of volcanic products (*49, 51, 52, 56*). For example, lavas produced from volcanoes located on extended lithosphere in the Nicaraguan graben are less silicic compared to those lavas produced on less extended lithosphere, and volcanoes located within the segments of extended lithosphere are larger than those located at segment boundaries (*51*).

There is structural evidence from several active and ancient arcs that volcanism is contemporaneous with normal faulting and subsidence. Many active volcanoes sit in depressions or fault-bounded grabens and are cut by steeply dipping faults that trend both parallel and transverse to the arc (*49, 57*). Syndepositional normal faulting and the distribution of sedimentary and volcanic units have also been interpreted as evidence for subsidence and deformation while the arc was active (*58*). Intrusion of magma into the crust can also produce extension on a local scale (*59*). However, the seismic data indicate that extension perpendicular to the arc is a regional scale phenomena, and is not simply related to the emplacement of magma bodies.

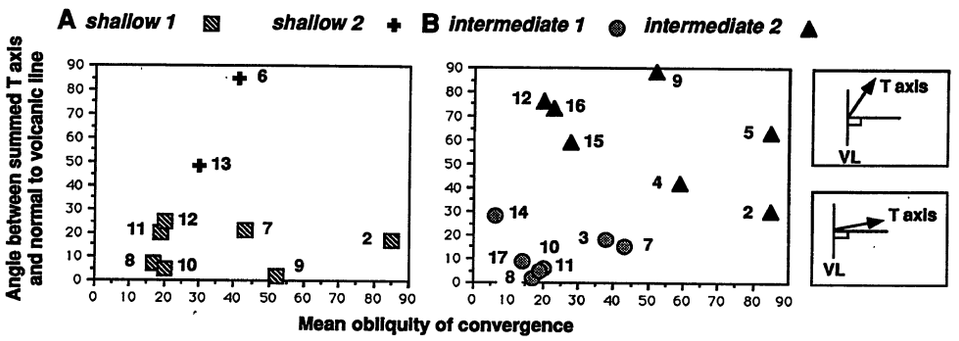

Fig. 8. Angle between the volcanic line and T axes of summed volcanic arc moment tensors versus mean obliquity of convergence. The four populations of volcanic arc earthquakes defined in Fig. 6 are schematically illustrated by the small map view insets that illustrate the orientation of the T axes relative to the volcanic line. The Shallow 1 convergent margin subregions possess a range of convergence obliquities; the two subregions in Shallow 2 have intermediate valued mean obliquities. The Intermediate 1 group has normal to intermediate obliquities, whereas the Intermediate 2 group has a wide range of values (Table 1).

Seismic Strain and Asthenospheric Corner Flow

The highly consistent orientation of seismic strain in the volcanic arc regions of many convergent margins suggests that an organized driving stress field is operating that is relatively independent of many of the geometrical parameters used to determine stress fields of convergent margins (*60*). In particular, the data imply that in-plate stresses generated as a result of coupling between the overriding and subducting plates may not be transmitted to the volcanic arc. A possible source of such a coherent strain field that is likely to operate at all active convergent margins is induced asthenospheric corner flow concentrated in the asthenosphere wedge under the volcanic arc region (Fig. 1) (*61*). Asthenosphere corner flow may also drive back arc extention (*12, 13*), although appropriately oriented absolute plate motions may be necessary to initiate spreading (*17*).

The magnitude of drag stresses generated on the base of overriding plate lithosphere by convecting asthenosphere are estimated to be about 3 to 5 MPa (*12*). If intermediate-depth volcanic arc earthquakes are indeed caused by stress concentrations where colder, stronger material is in contact with the edges of weak partially melted zones, these material discontinuities could be quite sensitive to small changes in tectonic stress. The consistent source orientation of these events would then be a result of the constrained flow patterns of the asthenosphere material in the corner above the slab. The interaction of the corner flow with the base of the arc lithosphere could also provide a source of tectonic stress that systematically orients the shallow crustal events relative to the arc as well. However, as mentioned above, magma fracturing, particularly at near-surface depths, could also play a role.

Some of the intermediate-depth volcanic arc events are located in the Wadati-Benioff zone of the subducting plate. In-plate stresses transmitted within the subducting slab, such as those generated by bending, could be responsible for some of the variations in source orientation observed for the events in the Intermediate 2 convergent margins. However, there is a suggestion of organization in the summed sources of Intermediate 2 margins because the P and T axes form girdles on the equal area projection (Fig. 6B). Although little work has been done on this problem, it is possible that interference of regional asthenospheric flow systems with local corner flow patterns could reorient the stress fields and cause scatter in the earthquake source orientations.

REFERENCES AND NOTES

1. Sediment accretion is not a universal process, and sediment subduction and even subduction erosion of the overriding plate are equally important [for example, R. von Huene, *Annu. Rev. Earth Planet. Sci.* **12**, 359 (1984)].
2. The backstop is a strong load-bearing member of the overriding plate and may consist of volcanic arc crust or lithified sediments of an older forearc [D. E. Byrne, D. M. Davis, L. R. Sykes, *Tectonics* **7**, 833 (1988)].
3. Most convergent margins show no active backarc tectonism. However, at some, backarc extension has resulted in the formation of hundreds of kilometers of new oceanic crust with magnetic lineations and spreading centers that appear to be similar to those at mid-ocean spreading ridges [for example, J. K. Weissel, *Phil. Trans. R. Soc. London Ser. A* **300**, 223 (1981)].
4. J. B. Gill, *Orogenic Andesites and Plate Tectonics* (Springer-Verlag, New York, 1981).
5. The Wadati-Benioff zone refers to earthquakes located in the subducting slab at depths greater than 60 or so kilometers. Shallow interplate shear-zone thrust earthquakes do not occur below that depth [J. Kelleher, J. Savino, H. Rowlett, W. McCann, *J. Geophys. Res.* **79**, 4889 (1974)].
6. D. Karig, *Annu. Rev. Earth Planet. Sci.* **2**, 51 (1974).
7. L. Ruff and H. Kanamori, *Phys. Earth Planet. Inter.* **23**, 240 (1980).
8. R. D. Jarrard, *Rev. Geophys.* **24**, 217 (1986).
9. S. Uyeda and H. Kanamori, *J. Geophys. Res.* **84**, 1049 (1979).
10. Examples include the Coulomb wedge model of deformation of accretionary prisms [D. Davis, J. Suppe, F. A. Dahlen, *ibid.* **88**, 1153 (1983)], the subduction channel model of a viscously deforming shear zone of variable thickness [R. L. Shreve and M. Cloos, *ibid.* **91**, 10229 (1986)], and finite element models such as in (*11*).
11. Analysis of viscoelastic finite-element models of subduction with an alternately locked and unlocked subduction fault suggest that the forearc experiences horizontal tectonic compression but that in the region of the volcanic arc, stresses may be either horizontal tension or compression [M. H. P. Bott, G. D. Waghorn, A. Whittaker, *Tectonophysics* **170**, 1 (1989)].
12. M. N. Toksoz and P. Bird, in *Island Arcs, Deep Sea Trenches, and Back-arc Basins*, M. Talwani and W. C. Pitmann III, Eds. (Maurice Ewing Series, vol. 1, American Geophysical Union, Washington, DC, 1977), pp. 379–393; N. H. Sleep and M. N. Toksoz, *Nature* **33**, 548 (1971).
13. M. N. Toksoz and A. T. Hsui, *Tectonophysics* **50**, 177 (1978).
14. Z. Garfunkel, C. A. Anderson, G. Schubert, *J. Geophys. Res.* **91**, 7205 (1986).
15. P. Molnar and T. Atwater, *Earth Planet. Sci. Lett.* **41**, 330 (1978); J. F. Dewey, *Geol. Assoc. Can. Spec. Pap. 20* (1980), p. 553.
16. This coupling force is also called the trench suction force [D. W. Forsyth and S. Uyeda, *Geophys. J. R. Astron. Soc.* **43**, 163 (1975)].
17. R. L. Carlson and P. J. Melia, *Tectonophysics* **102**, 399 (1984).
18. H. R. Shaw, in *Physics of Magmatic Processes*, R. B. Hargraves, Ed. (Princeton Univ. Press, Princeton, NJ, 1980), pp. 201–264; D. A. Spence and D. L. Turcotte, *J. Geophys. Res.* **90**, 575 (1985); B. Chouet and B. R. Julian, *ibid.*, p. 11187.
19. Relocation of the events can be performed if a detailed local Earth model is available [for example, E. R. Engdahl, N. H. Sleep, M. T. Lin, *Tectonophysics* **37**, 95 (1976)].
20. T. Yoshii, *ibid.* **55**, 349 (1979).
21. M. J. Carr and R. E. Stoiber, *Bull. Volcanol.* **37**, 326 (1973).
22. C. Blot, *J. Volcanol. Geotherm. Res.* **31**, 239 (1987).
23. S. R. McNutt, *ibid.*, p. 239.
24. A. I. Farberov and V. I. Gorelchik, *Bull. Volcanol.* **35**, 1 (1971).
25. A. Sugimura, *Zisin Jpn. Seismol. Soc.* **19**, 96 (1966).
26. An analysis of the frequency and location of intermediate-depth seismicity and volcanic activity for several circum-Pacific convergent margins suggested that convergent margins with high levels of seismicity at depths of 70 to 160 km but little volcanic activity had less melt present beneath the arc than those margins with low levels of seismicity but many active volcanoes [M. J. Carr, *J. Volcanol. Geotherm. Res.* **19**, 349 (1983)].
27. A spatial correlation of intermediate-depth earthquakes with active volcanoes has been demonstrated in Central America (*21*), New Hebrides and New Zealand (*22*), the Aleutians (*23*), and Kamchatka (*24*).
28. Seismic deformation represents only part of the total deformation at a convergent margin. For example, the ratio of seismic slip calculated from earthquakes located in the interplate shear zone to the amount of slip predicted by plate motion models suggests that half or more of total plate motion is aseismic, although the proportion varies considerably among different plate boundaries [H. Kanamori, in *Island Arcs, Deep Sea Trenches, and Back-arc Basins*, M. Talwani and W. C. Pitmann III, Eds. (Maurice Ewing Series, vol. 1, American Geophysical Union, Washington, DC, 1977), pp. 163–174].
29. The CMT solutions are published regularly in *Phys. Earth Planet. Inter.* [also see A. M. Dziewonski, T.-A. Chou, J. E. Woodhouse, *J. Geophys. Res.* **86**, 2825 (1981); (*30*)].
30. D. Giardini, *Geophys. J. R. Astron. Soc.* **77**, 883 (1984)].
31. M. I. Jost and R. B. Herrmann, *Seismol. Res. Lett.* **60**, 37 (1989); J. Jackson and D. McKenzie, *Geophys. J. R. Astron. Soc.* **93**, 45 (1988).
32. C. Frohlich and K. D. Apperson, *Tectonics*, in press.
33. C. Frohlich, M. A. Riedesel, K. D. Apperson, *Geophys. Res. Lett.* **16**, 523 (1989).
34. G. Ekstrom and A. M. Dziewonski, *Bull. Seismol. Soc. Am.* **75**, 23 (1985).
35. K. D. Apperson and C. Frohlich, *Eos* **69**, 1438 (1988).
36. V. V. Kostrov, *Izvestia Earth Phys.* **1**, 23 (1974).
37. The criteria for selection of convergent margins were: (i) active subduction of an oceanic plate of at least a few centimeters per year, (ii) at least three volcanoes with recorded eruptive activity within the last 1000 years [T. Simkin *et al.*, *Volcanoes of the World* (Smithsonian Institution, Washington, DC, 1981)], (iii) the occurrence of at least 10 earthquakes shallower than 200 km that could be identified as volcanic arc events, and (iv) the margin was farther than 2° from a triple junction, cusp, or other geometric complexity in the plate boundary. These criteria excluded margins such as the Philippines because of the complicated plate boundaries in the region and Ryuku because there were not enough earthquakes in the catalog for this margin.
38. The convergence rate and direction used to calculate the obliquity of convergence (Table 1) are taken from the NUVEL-1 plate motion model [C. DeMets, R. G. Gordon, D. F. Argus, S. Stein, *Geophys. J. Int.* **101**, 425 (1990)]. The motion of the Philippine Sea plate relative to the Eurasian and Pacific plates is taken from B. Ranken, R. K. Cardwell, and D. E. Karig [*Tectonics* **3**, 555 (1984)]. The obliquity of convergence is the angle between the direction of convergence and the normal to the plate boundary.
39. Sources of error in earthquake locations listed in the CMT catalog include errors in the reported epicentral coordinates and in the calculated CMT focal depths. CMT depths greater than 40 km can have an error of a few kilometers, but the CMT inversion scheme is poorly constrained for focal depths less than about 10 km [for example (*30*)]. Because I relied primarily on source characteristics to separate groups of similar events, I did not relocate the earthquakes used in this study.
40. I took the location of the plate boundaries from data supplied by the Paleo-Oceanographic Mapping Project (POMP) group at the University of Texas at Austin. This group placed convergent margin plate boundaries along the bathymetric low of the trench.
41. The location of the cross sections are marked on Fig. 4 by heavy lines. Each cross section is enclosed by a box 200 km deep and approximately 500 km wide with lateral boundaries that are defined by recent active volcanism, changes in amount of seismicity, and changes in the orientation of the volcanic line azimuth. Earthquakes in each box are projected onto the plane of the cross sections. The cross sections are

oriented perpendicular to the volcanic line, whose direction is determined by a least squares fit to the volcanoes in each subregion. The bathymetrically defined plate boundary may not actually represent the boundary between the plates because variations in amount of sediment supplied to the slope and trench can affect bathymetry. The volcanic line located within the crystalline part of the overriding plate may be a more fundamental marker of the orientation of the boundary between the plates. Because of possible errors incurred by the use of a bathymetrically defined plate boundary, the obliquity (*38*) is calculated with the normal direction to the volcanic line. However, the bathymetrically-defined plate boundary is a useful geographic marker. For regions such as Kermadec or central Chile without substantial volcanic activity in the last 1000 years, the sections are oriented normal to the plate boundary.

42. Hamilton has previously suggested that all volcanic arcs are extensional as a result of trench suction forces on the overriding plate [W. B. Hamilton, in *Metamorphism and Crustal Evolution of the Western United States*, Rubey Volume III, W. G. Ernst, Ed. (Prentice Hall, New Jersey, 1988), pp. 1–40; *Geol. Soc. Am. Bull.* **100**, 1503 (1988)].
43. Although the high values of f_{ndc} for summed sources in several subregions might suggest that many of the individual events are also anomalous, the mean value of f_{ndc} of individual events is generally much lower than the value of f_{ndc} of the sum. Recall that a non–double couple summed source can be created by adding together two appropriately oriented double couples (Fig. 2). Frohlich and Apperson (*32*) analyzed shallow earthquakes (<50-km depth) from the CMT catalog that were located at various types of plate boundaries (spreading ridge, transform boundary, or subduction zone) and found that anomalous events with high values of f_{ndc} (>0.2) occur in all tectonic environments but in rather low proportions relative to other events. A study of deep non–double couple earthquakes at subduction zones suggests that they are likely due to source complexity in space and time (*33*). A few events with large amounts of non–double couple component have been connected to magma fracturing [for example, B. R. Julian and S. A. Sipkin, *J. Geophys. Res.* **90**, 11155 (1985)], but such events are quite shallow and would not be resolved in the Harvard CMT catalog.
44. R. D. Jarrard, *Tectonophysics* **132**, 89 (1986).
45. It is unlikely, however, that such decoupling will be efficient or complete [for example, R. McCaffrey, *Eos* **71**, 1590 (1990)].
46. T. J. Fitch, *J. Geophys. Res.* **77**, 4432 (1972).
47. P. Huchon and X. Le Pichon, *Geology* **12**, 668 (1984).
48. It has been proposed that large strike-slip faults are inherently weak, and thus force reorientation of principal stresses parallel and perpendicular to the fault trace [M. D. Zoback *et al.*, *Science* **238**, 1105 (1987)]. However, it should also be considered that the orientation of principal stresses relative to a fault can only be predicted for initial failure. Once a discontinuity exists, principal stresses are not constrained by simple faulting theory.
49. B. Burkart and S. Self, *Geology* **13**, 22 (1985).
50. A. F. Glazner and W. Ussler III, *J. Geophys. Res.* **94**, 7952 (1989); D. R. Baker, *Geology* **15**, 496 (1987).
51. M. J. Carr, *J. Volcanol. Geotherm. Res.* **20**, 231 (1984).
52. B. S. Singer and J. D. Myers, *Geology* **18**, 1050 (1990).
53. R. J. Arculus, in *Formation of Active Ocean Margins*, N. Nasu *et al.*, Ed. (Terra Scientific, New York, 1985), pp. 367–397.
54. B. S. Singer, J. D. Myers, S. R. Linneman, C. L. Angevine, *J. Volcanol. Geotherm. Res.* **37**, 273 (1989).
55. B. D. Marsh, *Am. J. Sci.* **86**, 808 (1982).
56. Hughes and others correlated chemistry and petrology with the segmented arc in the Cascades, noting that volcanoes located near segment boundaries produce a great variety of lava types and eruption styles [J. M. Hughes, R. E. Stoiber, M. J. Carr, *Geology* **8**, 15 (1980)].
57. For example, studies have been conducted on active volcanoes in Kamchatka [E. N. Erlich, *Bull. Volcanol.* **42**, 13 (1979)], Central America (*21*), the Oregon High Cascades [G. A. Smith, *Eos* **70**, 1299 (1989)], and the Nicaraguan arc [G. Dengo, O. Bohnenberger, S. Bonis, *Geol. Rundsch.* **59**, 1215 (1970)]. Drilling in the Izu-Bonin forearc and volcanic arc produced evidence for rifting associated with volcanism that split the older Eocene forearc high in front of the present arc [K. Fujioka, B. Taylor, T. Janecek, and Leg 126 Shipboard Scientific Party, *Nature* **342**, 18 (1989)].
58. Busby-Spera has suggested the early Mesozoic arc in the southwestern United States subsided rapidly during arc activity [C. Busby-Spera, *Geology* **16**, 1121 (1988)]. She postulated that wide areal distribution of cratonic sediments over the arc is evidence for a long-lived depression in which the arc was located. Tobisch and others proposed that the Cretaceous Sierra Nevada arc was extensional during arc activity on the basis of rotation and deformation of related sedimentary and volcanic units [O. T. Tobisch, J. B. Saleeby, R. S. Fiske, *Tectonics* **5**, 65 (1986)]. On the basis of the similar sediment distribution and deformation in the Oregon High Cascades, Smith and others also proposed that late Miocene volcanism there was accompanied by extension [G. A. Smith, L. W. Snee, E. M. Taylor, *Geology* **15**, 389 (1987)].
59. S. M. Cather, *Geol. Soc. Am. Bull.* **102**, 1447 (1990).
60. Carr (*26*) previously suggested that variables such as age and dip of the subducting slab do not appear to affect the stress field in the volcanic arc region.
61. Extension in the volcanic arc region may be the normal mode of behavior, yet there are situations in which this tectonic stress field can be greatly perturbed, at least at continental convergent margins. Flat slab subduction beneath continental overriding plates can displace local asthenosperic corner flow and arc magmatism hundreds of kilometers, and even shut the arc off. Examples include central Chile today [R. W. Allmendinger *et al.*, *Tectonics* **9**, 789 (1990)], and the Cretaceous convergent margin of western North America [P. W. Lipman, H. J. Prostka, R. L. Christiansen, *Science* **174**, 165 (1971); (*42*)]. Short-lived fold and thrust belts in foreland basins behind the volcanic arc [W. R. Dickinson, in *Island Arcs, Deep Sea Trenches, and Back-arc Basins*, M. Talwani and W. C. Pitmann III, Eds. (Maurice Ewing Series, vol. 1, American Geophysical Union, Washington, DC, 1977), pp. 33–40] appear to have been contemporaneous with displaced arc magmatism and flat slab subduction at both the Cretaceous North American margin and in South America [T. E. Jordan and R. W. Allmendinger, *Am. J. Sci.* **86**, 737 (1986)]. Tremendous thickening of the overriding plate and unusually high topography have also been linked to flat slab subduction [B. L. Isacks, *J. Geophys. Res.* **93**, 211 (1988)]. Although there is still considerable controversy surrounding the mechanism by which a subducting slab can flatten to near horizontal, numerical models clearly indicate that flat slab subduction can dramatically, and perhaps rather quickly, alter the tectonic stress fields and deformation styles of the overriding plate [P. Bird, *Science* **239**, 1501 (1988)].

62. I thank L. Davis, D. Smith, C. Frohlich, and particularly M. Cloos for their comments. I also thank the many encouraging persons on both sides of the Pacific with whom I discussed this project. This research was partially funded by a National Science Foundation Graduate Fellowship.